sciendo

Civil and Environmental Engineering
Vol. 16, Issue 1, 86-106, DOI: 10.2478/cee-2020-0010

DETERMINATION OF MECHANICAL PROPERTIES OF FIBER REINFORCED CONCRETE FOR NUMERICAL MODELLING

Z. MARCALIKOVA[1,*], R. CAJKA[1]

[1] Department of Structures, Faculty of Civil Engineering, VSB-Technical University of Ostrava, Ludvíka Podéště 1875/17, 708 33 Ostrava-Poruba, Czech Republic.
[*] corresponding author: zuzana.marcalikova@vsb.cz.

Abstract

The paper deals with the determination of mechanical properties of fiber reinforced concrete in dependence on various dosages and recipe of concrete. The mechanical properties were determined for the default recipe of concrete, where the individual variants differ in the amount of fibers. The fibers dosing was 0, 25, 50 and 75 kg/m^3. At the highest dosage of 75 kg/m^3, the recipe is optimized with regard to the microstructure of the concrete. In the experimental program were determined compressive strength, modulus of elasticity, split tensile strength, flexural tensile strength and load-displacement diagram. The flexural tensile strength was determined based on a three-point and four-point bending test. Based on the evaluated data, the uniaxial tensile strength and the functional dependence for the resultant recipe of concrete with a dosage of 75 kg/m^3 is with respect of the increasing importance and application of numerical modelling of building structures, the analysis is performed using non-linear calculation. The aim was to simulate the performed laboratory test and appropriately approximate the specific input parameters of the fiber reinforced concrete for nonlinear analysis.

Keywords:

Fiber;
Concrete;
Mechanical properties;
Numerical modelling;
Flexural strength.

1 Introduction

Fiber reinforced concrete exists in a whole series variant [1]. For example, reinforced concrete with steel 3D fibers is widely used in construction where a static function or higher ductility of the construction is also required. These are mostly industrial floors [2, 3], storage areas or parking spaces. Fiber reinforcement eliminates a number of disadvantages of traditional concrete, where the design of industrial floors itself involves a closer knowledge of the qualitative parameters [4], in particular the mechanical properties [5, 6], which are determined by specialized laboratory tests [7-9]. Important material properties are in particular: compressive strength, modulus of elasticity, split tensile strength, flexural tensile strength and fracture energy. These material properties are also important for the numerical modelling of fiber reinforced concrete structures. However, attention must also be paid to specific input parameters. These parameters depend on the selected numerical methods and the material model of the concrete [10-15]. Testing of fiber reinforced concrete and its properties is very demanding and there is often a large dispersion of measured values [16]. This is influenced by the distribution of the fiber in the concrete mix, compaction and water-cement ratio Therefore, it is also important to optimize the individual components of fiber reinforced concrete, where their ratio affects the resulting mechanical properties, but also the workability and pumpability of concrete [17]. For a number of areas, a much of design recommendations and standards can be found, RILEM [18], BS [19], DafStB [20] and Model Code 2010 [21]. A specific problem is the testing and determination of tensile strength and fracture energy [22-25].

For good operation and economy of the proposal is an important fiber dosing optimization and appropriate choice of concrete recipe. This then allows us to reduce the thickness of the structure, reduce the amount of classical reinforcement compared to the solution of reinforced concrete. Specific problems in which fiber reinforced concrete is applied include, in particular, solving the role of slab in

interaction with the subsoil [26, 27] or the problem of punching in concrete [28], shear failure [29]. By adding fibers to the concrete mixture, the concrete better resists the bending tensile stress even after the formation of the first micro-cracks. The toughness of the material increases. However, numerical modelling is now used to optimize structural design. These include finite element method [30, 31] and nonlinear analysis. However, wider application in design is prevented by knowledge of detailed input parameters for the creation of nonlinear concrete models.

2 Numerical modelling for FRC

Modelling of fiber reinforced concrete construction is performed using nonlinear analysis of structures and finite element method [30]. There are a number of commercial and research SW and algorithms [32]. The biggest qualitative differences in analyses of fiber reinforced concrete structures are most often in used material models and their theoretical basis.

It is common for the analysis itself to use the finite element method [30, 31]. The method can be included in well algorithmizable numerical methods. The calculation model composed of finite elements. Finite elements most often have the shape of a beam and a plate or spatial element, see. Fig.1. The finite element method is based on energy principles. The principle of minimum potential energy is used, which is used to solve the equilibrium conditions on each element:

$$\Pi = \Pi_e + \Pi_i = min., \tag{1}$$

where Π_e is the potential energy of external forces and Π_i is potential energy of internal forces.

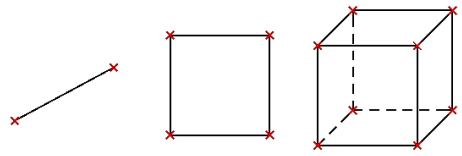

Fig. 1: Finite elements.

The finite element method has different variants, most often the deformation variant is applied, which is governed by the Lagrange variation principle. Solved system of linear equations and FEM basic equation is given by the relation:

$$\mathbf{K} \cdot \mathbf{u} = \mathbf{F}, \tag{2}$$

where **K** is the stiffness matrix of the construction, **u** is a vector of unknown displacements and **F** is a vector of nodal loads.

The finite element method can be used in nonlinear analysis, where the calculation is divided into the incremental solution in the most widespread Newton-Raphson variant:

$$\mathbf{K(u)} \cdot \mathbf{\Delta u_i} = \mathbf{\Delta F_i}, \tag{3}$$

where **K(u)** is the stiffness matrix of the construction dependent on the displacement vector u, $\mathbf{\Delta u_i}$ is the deformation increment for the load step $\mathbf{\Delta F_i}$. A graphical representation of the Newton-Raphson method is shown in Fig. 2.

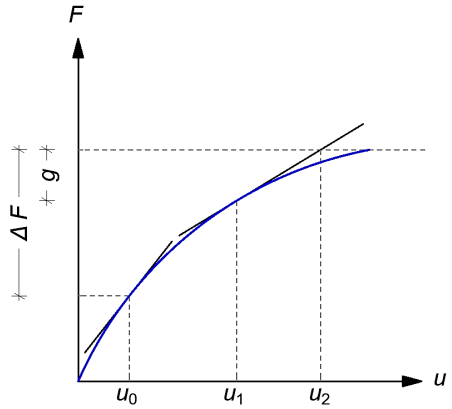

Fig. 2: Newton-Raphson method.

Before modelling of fiber reinforced concrete construction, however, it is necessary to determine the input parameters characterizing the behavior of fiber reinforced concrete - material model. There are several approaches for example, it belongs here use of nonlinear fracture mechanics in combination with the crack width method and the cracked crack concept [12]. The input parameters are tensile strength, fracture energy and the shape of the curve indicating the relationship between stress and crack opening [33]. A typical approximation of concrete softening after crack formation is shown in Fig. 3.

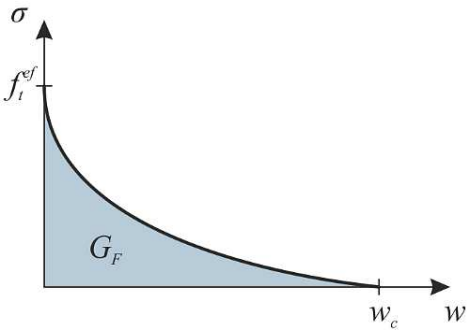

Fig. 3: Relationship between stress and crack width – SBETA - concrete [33].

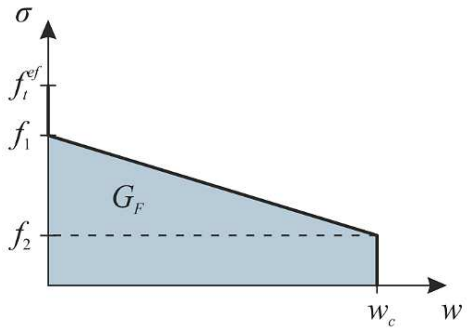

Fig. 4: Relationship between stress and crack width [33].

In the case of the exponential curve, the relationship between stress and crack width can be expressed:

$$\frac{\sigma}{f_t^{ef}} = \left\{1 + \left(c_1 \frac{w}{w_c}\right)^3\right\} exp\left(-c_2 \frac{w}{w_c}\right) - \frac{w}{w_c}(1 + c_1^3) exp(-c_2), \tag{4}$$

which was subsequently transformed based on shape experiments:

$$w_c = 5.14 \cdot \frac{G_f}{f_t^{ef}}. \tag{5}$$

In the case of fiber reinforced concrete, the behavior is shown in Fig. 4. The softening parameters for the course shown in Fig. 4 can be determined according to:

$$c_1 = \frac{f_1}{f_t^{ef}}, \tag{6}$$

$$c_2 = \frac{f_2}{f_t^{ef}}, \tag{7}$$

$$w_c = \frac{2G_f}{f_1 + f_2}. \tag{8}$$

The correlation coefficients of softening are different depending on the type of fiber and concrete used. The possibility of describing tensile softening depends primarily on the amount of available information from the experiments. In general, the softening of reinforced concrete can be very well modeled using the diagram in Fig. 5.

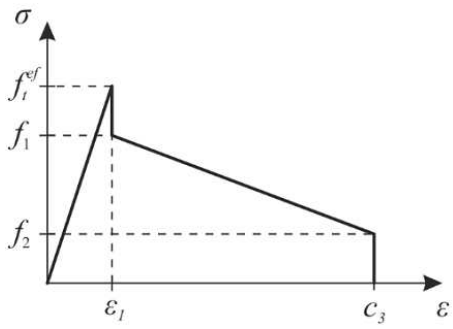

Fig. 5: Dependencies between strain and tensile stress [33].

Possible approaches to modelling of fiber reinforced concrete in nonlinear tasks also include the possibility of creating a composite using a material model for concrete (matrix) and a model of reinforcement. The model of reinforcement is shown in Fig. 6. For the model, the stiffness matrix of reinforcement material for individual directions of reinforcement is assembled. The stiffness of each reinforcement direction can be described by the material stiffness matrix:

$$\mathbf{D}_{s,i} = \begin{bmatrix} pE_{s,i} & 0 & 0 \\ 0 & 0 & 0 \\ 0 & 0 & 0 \end{bmatrix}, \tag{9}$$

where p is the degree of reinforcement determined from the ratio of the reinforcement area to the total cross - sectional area (finite element) and $E_{s,i}$ is the modulus of elasticity of the material. The material stiffness matrix for the 2D problem is further transformed into the relevant direction by the equation:

$$\mathbf{D}_s = \mathbf{T}_\sigma^{-1}\mathbf{D}_{S,x}\mathbf{T}_\varepsilon, \tag{10}$$

where $\mathbf{T_\sigma^{-1}}$ is the transformation matrix, $\mathbf{D_{S,x}}$ is the stiffness matrix of reinforcement and $\mathbf{T\varepsilon}$ is a transformation matrix.

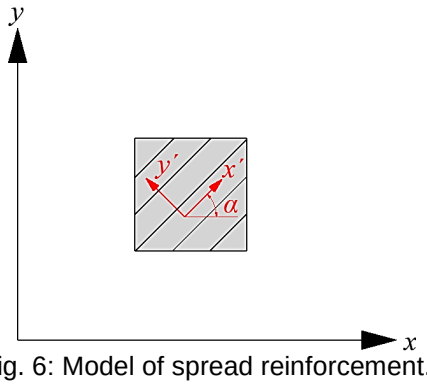

Fig. 6: Model of spread reinforcement.

Transformation matrices are defined by:

$$\mathbf{T}_{\sigma} = \begin{bmatrix} \cos^2\alpha & \sin^2\alpha & 2\cdot\cos\alpha\cdot\sin\alpha \\ \sin^2\alpha & \cos^2\alpha & -2\cdot\cos\alpha\cdot\sin\alpha \\ -\cos\alpha\cdot\sin\alpha & \cos\alpha\cdot\sin\alpha & \cos^2\alpha-\sin^2\alpha \end{bmatrix} \tag{11}$$

and

$$\mathbf{T}_{\varepsilon} = \begin{bmatrix} \cos^2\alpha & \sin^2\alpha & \cos\alpha\cdot\sin\alpha \\ \sin^2\alpha & \cos^2\alpha & -\cos\alpha\cdot\sin\alpha \\ -2\cdot\cos\alpha\cdot\sin\alpha & 2\cdot\cos\alpha\cdot\sin\alpha & \cos^2\alpha-\sin^2\alpha \end{bmatrix}. \tag{12}$$

For a 3D task, the procedure is analogous. The stiffness of the reinforcement is added to the stiffness matrix of material **D** for concrete. The resulting material stiffness matrix has the form:

$$\mathbf{D} = \mathbf{D}_c + \sum_{i=1}^{n} \mathbf{D}_{s,i} \ , \tag{13}$$

where $\mathbf{D_C}$ is the stiffness matrix of concrete and $\mathbf{D_{s,i}}$ is the reinforcement stiffness matrix in individual directions.

The model of spread reinforcement assumes perfect interaction of reinforcement with concrete. This approach will be used in case of non-linear analysis.

3 Fiber-Reinforced Concrete

A total of 5 concrete mixtures were tested, which differed mainly by the dosing with the content of scattered reinforcement in the variants 0, 25, 50, 75 kg/m^3. The last dosage of 75 k/m^3 was carried out in two versions of the recipe. The proportion of individual components in concrete is shown in Table 1.

Table 1: Material properties of concrete.

Consistency	S3
Cement	CEM I
Minimum cement content	300 kg
Water-cement ratio: v/c	0.6
Fine aggregate *	870 kg
Coarse aggregate **	970 kg
Water	189 l
Plasticizer	2.9 l
Notes: * mining aggregate; ** mining aggregate (maximum aggregate size of 16 mm)	

As reinforcement were used fibers Dramix® 3D 65/60 BG [34]. Material and mechanical properties of fibers are given in Table 2. It was about the fibers with bends with the shape shown in Fig. 7. In the case of concrete with fibers dosing of 75* kg/m^3, the original recipe was modified according to Table 3.

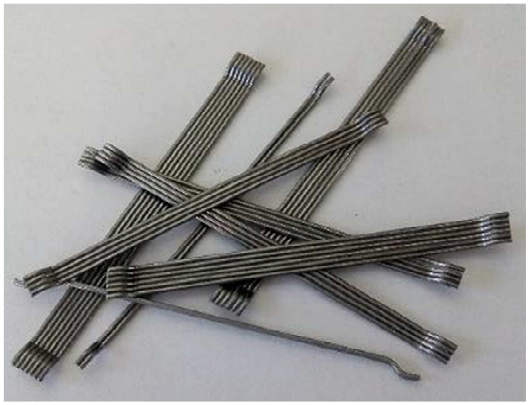

Fig. 7: Fiber Dramix® 3D 65/60 BG.

Table 2: Material properties of Dramix® 3D 65/60 BG.

Fiber shape	Hooked ends
Bundling	Glued
Coating	-
Length [mm]	60
Diameter [mm]	0.9
Aspect ratio	67
Modulus of elasticity [GPa]	200

Table 3: Modified recipe for fibers dosing 75* kg/m^3.

Consistency	S3
Cement	CEM I
Minimum cement content	320 kg
Water-cement ratio: v/c	0.625
Fine aggregate *	945 kg
Coarse aggregate **	970 kg
Water	200 l
Plasticizer	3.2 l
Notes: * mining aggregate; ** mining aggregate (maximum aggregate size of 16 mm)	

4 Recipe concrete

Adding fibers to concrete there is a change the microstructure of the material. This is then significantly affected for higher dosage cases where mechanical properties can also be negatively affected. By adjusting the recipe, which takes into account the content of fibers in the concrete, an optimal increase of the decisive strengths can be achieved. These are mainly split tensile strength and flexural tensile strength. With regard to previous research and experience, the fiber reinforced concrete recipe for higher fiber dosing has been modified to maintain optimal microstructure and connection of the individual components. The mechanical properties for the modified recipe are indicated by an asterisk in the graphs, i.e. 75* kg/m^3. The modified recipe is described in more detail in Chapter 3 in Table 3.

By adjusting the recipe, the tensile strengths increased significantly. The split tensile strength for dosing 75 kg/m^3 and the original recipe was 2.66 MPa. This strength was increased to 3.64 MPa for a modified recipe. The increase in split tensile strength compared to the unchanged recipe was 37 %. From the three-point bend test, the bending strength for the unchanged recipe was 4.31 MPa and for the changed recipe 5.02 MPa. The increase in flexural tensile strength by three-point test was 17 %. The flexural tensile strength determined based on of the four-point test for the unchanged recipe was 4.49 MPa and for the changed recipe 6.48 MPa. In this case, the strength increases by up to 44 %. A graphical representation of the basic mechanical properties is shown in Fig. 8 and tensile strengths in Fig. 9.

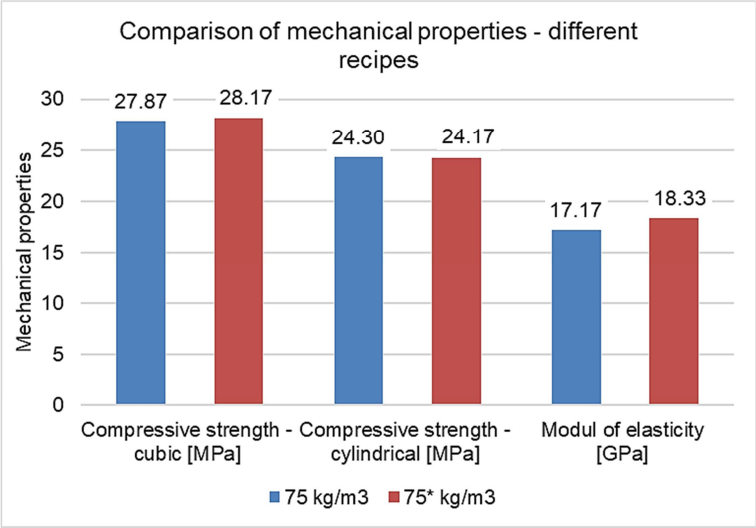

Fig. 8: Comparison of basic mechanical properties – different recipe.

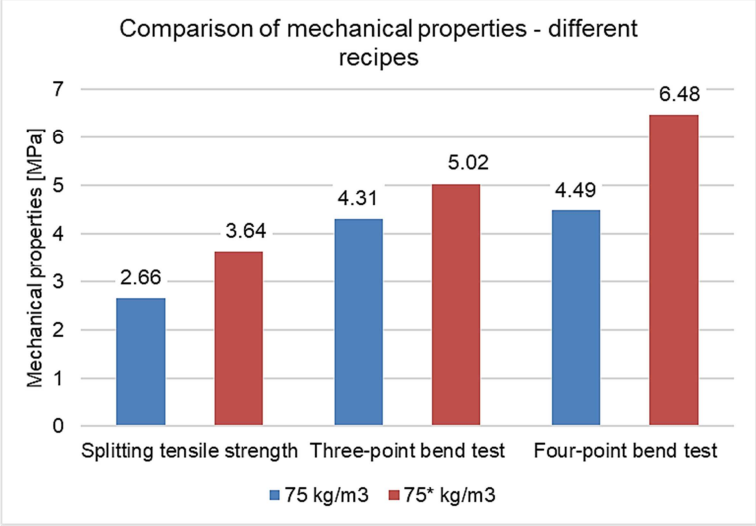

Fig. 9: Comparison of tensile properties – different recipe.

5 Mechanical properties of FRC

Based on the performed tests, the data were processed using regression analysis for select mechanical properties.

5.1 Compressive strength and modulus of elasticity

Testing of the compressive strength of concrete was carried out at the age of 28 days on cubes with dimensions 150 x 150 mm and on cylinders Ø 150 x 300 mm. A total of 12 test specimens, 6 cubes and 6 cylinders were concreted for each recipe. Compressive strength was determined from the relationship:

$$f_c = \frac{F_{max}}{A}, \tag{14}$$

where F_{max} is load size of failure of the test specimen and A area of test sample. The test scheme for determining the compressive strength is shown in Fig. 10.

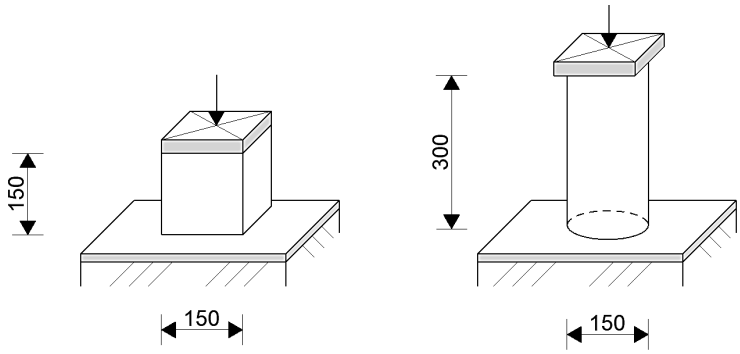

Fig. 10: Test scheme for compressive: cubic 150 x 150 x 150 mm (left), cylindrical Ø 150 x 300 mm (right).

Modulus of elasticity *E* was tested on cylinders with a diameter of 150 and height 300 mm according to the relation:

$$E = \frac{\Delta\sigma}{\Delta\varepsilon} = \frac{\sigma_a - \sigma_b}{\varepsilon_a - \varepsilon_b}\ , \tag{15}$$

where σ_a is upper loading stress in N/mm^2, σ_b = 0,5 is the basic loading stress in N/mm^2, ε_a is the average strain at upper load stress and ε_b is the average strain at the lower load stress.

The resulting mechanical properties are shown in Table 4. Fig. 11 shows graphically the resultant values of compressive strengths on cubes and cylinders. Fig. 12 is a graphical representation of static modulus of elasticity.

Table 4: Basis mechanical properties.

Mechanical properties	**Amount of fibers [kg/m^3]**				
	0	25	50	75*	75
Compressive strength – cubic $f_{c,cube}$ [MPa]	24.09	26.49	31.26	28.17	27.87
Compressive strength – cylindrical $f_{c,cyl}$ [MPa]	20.92	21.88	25.71	24.17	24.30
Modulus of elasticity *E* [GPa]	18.50	18.50	19.50	18.33	17.17

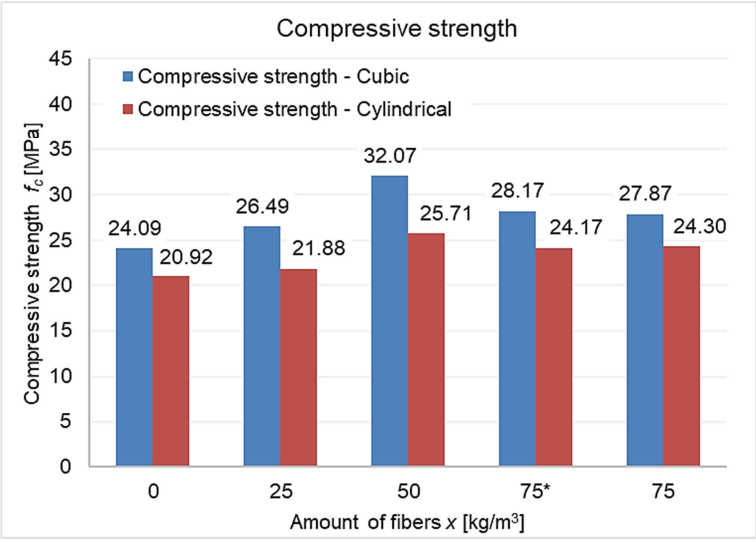

Fig. 11: Compressive strength.

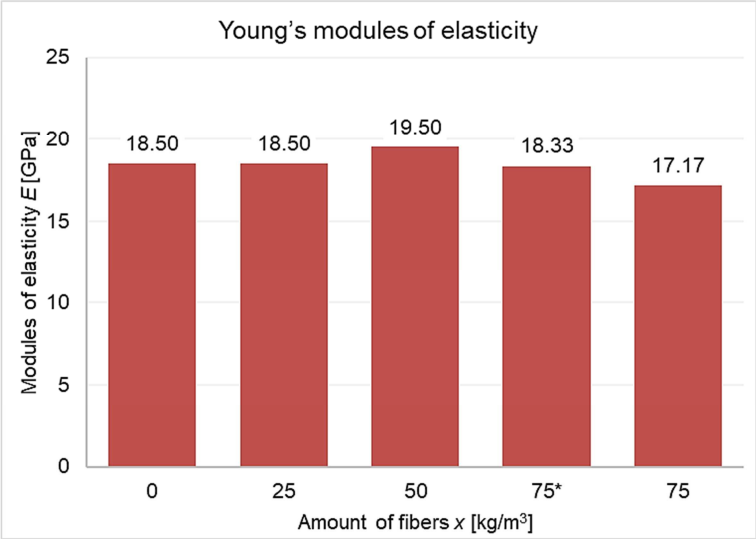

Fig. 12: Modulus of elasticity.

The functional dependence of compressive strength on the amount of fibers in concrete for unchanged recipe was determined (Fig. 13.), which is governed by the relation:

$$f_{c,cube} = 0.1468\,x + 24.09 \quad (R^2 = 0.9396), \tag{16}$$

$$f_{c,cyl} = 0.0843\,x + 20.92 \quad (R^2 = 0.8722), \tag{17}$$

where x is the amount of fibers in kg/m^3.

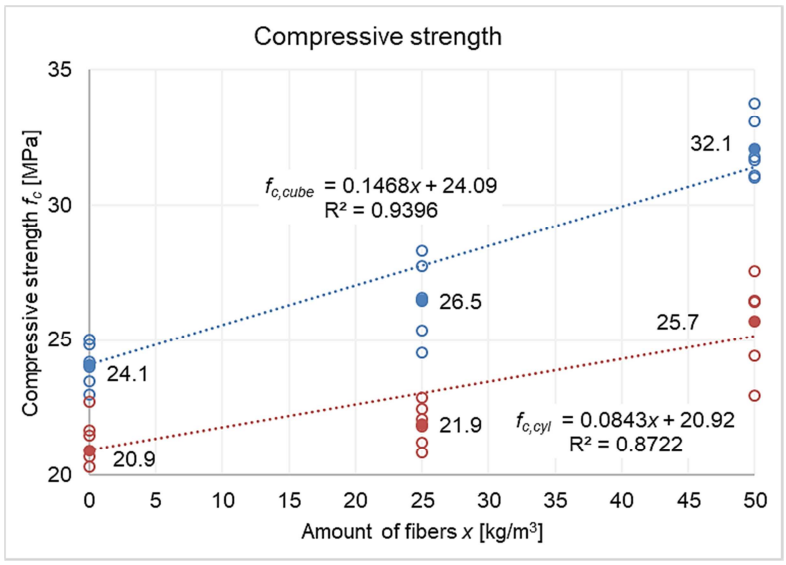

Fig. 13: Functional dependence - compressive strength.

5.2 Splitting tensile strength

This type of test was performed on cubes measuring 150 x 150 x 150 mm. The test scheme is shown in Fig. 14. The split tensile strength was determined according to the formula:

$$f_{ct,sp} = \frac{2 \cdot F}{\pi \cdot l \cdot d}, \tag{18}$$

where F is the maximum failure load of the sample, l is the length of the contact line and d is the split dimension of the sample.

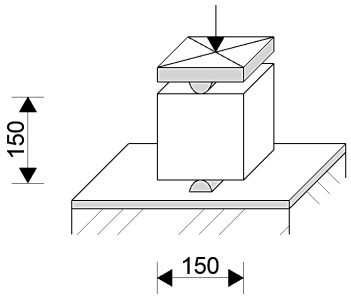

Fig. 14: Test scheme for splitting tensile strength.

The resulting functional dependence is shown in Fig. 15 and is governed by the relation:

$$f_{c,sp} = 0.0166\,x + 2.27 \quad (R^2 = 0.858), \tag{19}$$

where x is the amount of fibers in kg/m^3.

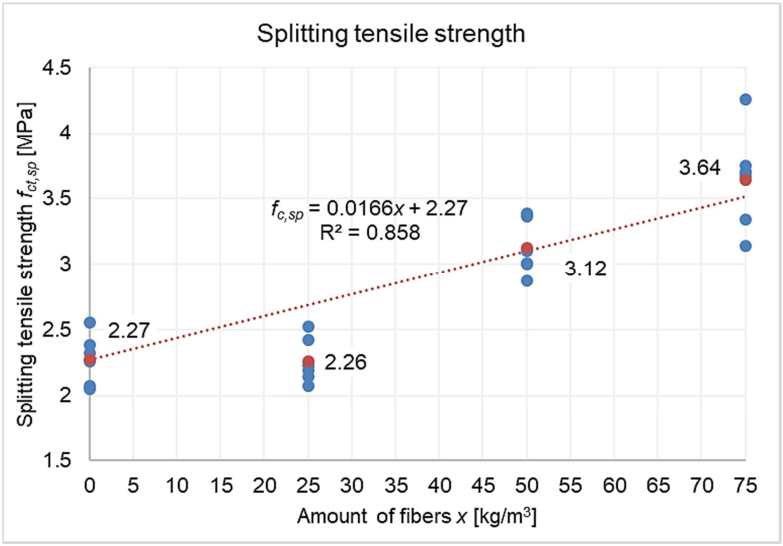

Fig. 15: Functional dependence - splitting tensile strength.

5.3 Bending tensile strength

The essence of the test was to determine the flexural tensile strength $f_{ct,fl}$ and to determine the LD diagram. Two types of tests were performed:

• Three-point bending test on beams of 150 x 150 x 700 mm with a 50 mm center notch and a 600 mm span. The test layout is shown in Fig. 16.

• Four-point bending test on beams of 150 x 150 x 600 mm without notch. The test layout is shown in Fig. 17.

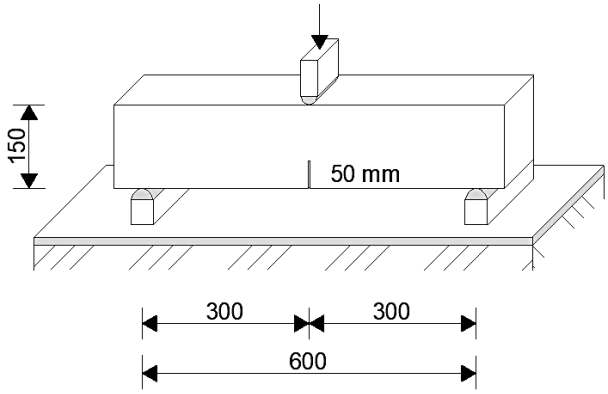

Fig. 16: Test scheme for three-point bending test.

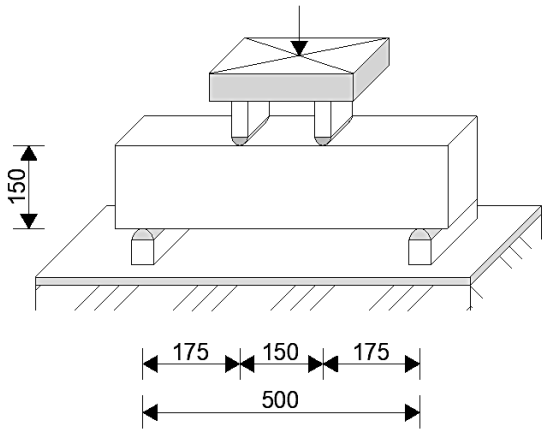

Fig. 17: Test scheme for four-point bending test.

A total was concreted of 12 samples for the three-point bending test and 12 samples for the four-point bending test. Each series of samples differed in the fibers content in the concrete and each contained 3 test specimens.

Bending tensile strength $f_{ct,fl}$ can be calculated to the formula for:

• Three-point bending test:

$$f_{c,fl} = \frac{3 \cdot F \cdot L}{2 \cdot b \cdot (h - a_0)^2}, \tag{20}$$

• Four-point bending test:

$$f_{c,fl} = \frac{6 \cdot F \cdot e}{2 \cdot b \cdot h^2}, \tag{21}$$

where F is the maximum load; L, b and h are the dimensions: span, width and height of the cross-section, a_0 is the notch height and e is the distance between support and force.

Based on the measured data, the bending tensile strength was evaluated (Table 5). Graphically, the resulting values are shown in Fig. 18 and 19.

• Three-point bending test:

$$f_{c,fl} = 0.0153\,x + 3.74 \quad (R^2 = 0.9476), \tag{22}$$

• Four-point bending test:

$$f_{c,fl} = 0.0418\,x + 2.75 \quad (R^2 = 0.8192), \tag{23}$$

where x is the amount of fibers in kg/m^3.

Table 5: Mechanical properties [MPa].

Type of test	**Amount of fibers [kg/m^3]**				
	0	25	50	75*	75
Splitting tensile strength	2.27	2.26	3.12	3.64	2.66
Four-point bend test	2.75	3.99	3.86	6.48	4.49
Three-point bend test	3.74	4.05	4.35	5.02	4.31

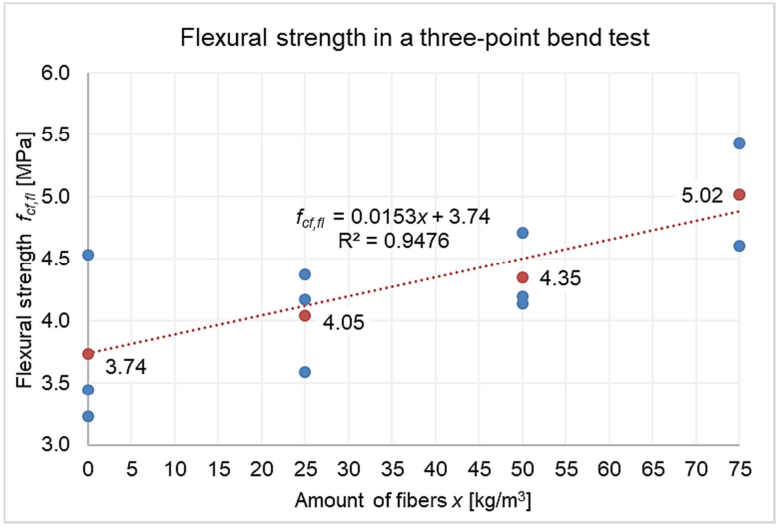

Fig. 18: Functional dependence - flexural strength in a three-point bend test.

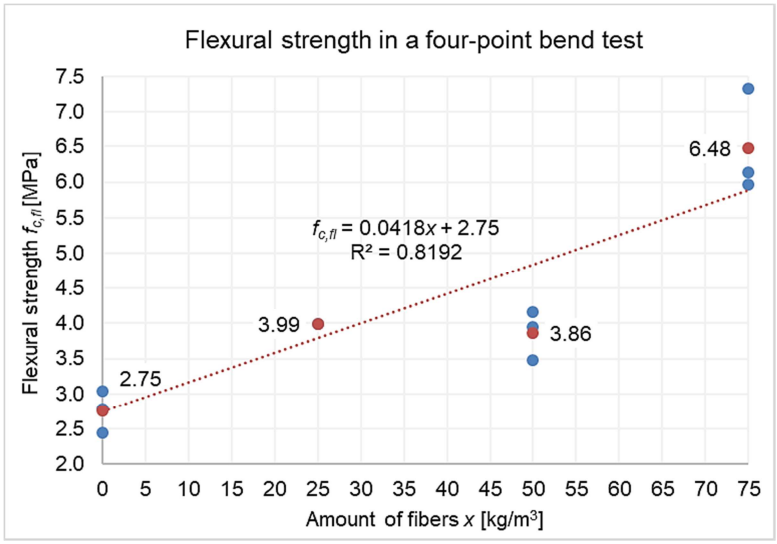

Fig. 19: Functional dependence - flexural strength in a four-point bend test.

The LD diagram for the three-point test is shown in Fig. 20 and for the four-point test in Fig. 21. Fig. 20 and Fig. 21 show a significant influence of the fibers content in concrete on the shape of the load-displacement diagram and also on the residual tensile strength and fracture energy, which are important for the modelling of fiber reinforced concrete structures, but cannot be used directly.

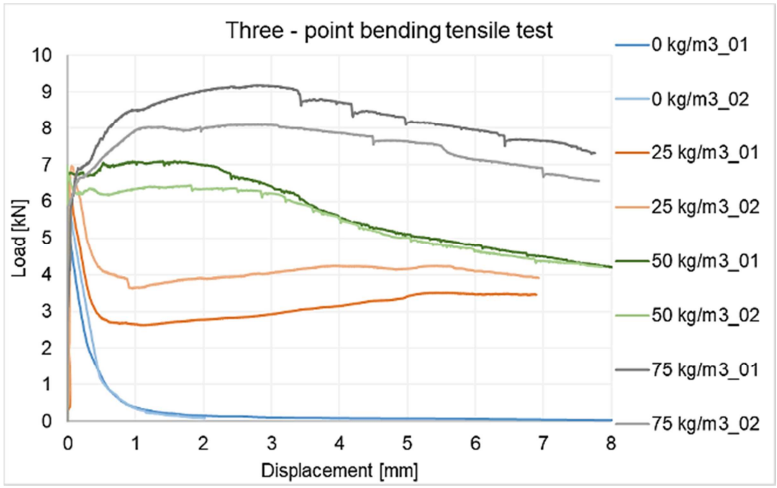

Fig. 20: LD diagram for three-point bending test.

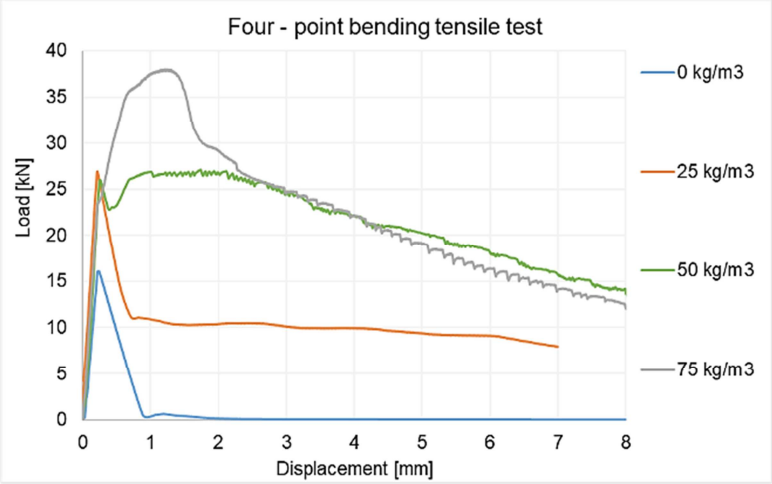

Fig. 21: LD diagram for four-point bending test.

5.4 Uniaxial tensile strength

A uniaxial tensile strength comparison was also performed based on all tensile tests. The uniaxial tensile strength value from the splitting tensile strength test as:

$$f_{ct} = f_{ct,sp}\,, \tag{24}$$

or by recalculating the bending tensile beam test using the formula:

$$f_{ct} = \frac{f_{ct,fl}}{1.65}\,, \tag{25}$$

Resulting values of uniaxial tensile strengths are shown in Table 6 and graphically illustrated in Fig. 22.

Table 6: Uniaxial tensile strength [MPa].

Uniaxial tensile strength	**Amount of fibers [kg/m^3]**				
	0	25	50	75*	75
Splitting tensile strength	2.27	2.26	3.12	3.64	2.66
Four-point bend test	1.67	2.42	2.34	3.93	2.72
Three-point bend test	2.27	2.45	2.64	3.04	2.61

The functional dependence between the uniaxial tensile strength and the dosing of fibers in concrete is governed by the relation, which is determined by:

- Splitting tensile strength test:

$$f_{ct} = 0.0166\,x + 2.27 \quad (R^2 = 0.858), \tag{26}$$

- Three-point bending test:

$$f_{ct} = 0.092\,x + 2.27 \quad (R^2 = 0.9462), \tag{27}$$

- Four-point bending test:

$$f_{ct} = 0.0253\,x + 1.67 \quad (R^2 = 0.8189), \tag{28}$$

where x is the amount of fibers in kg/m^3.

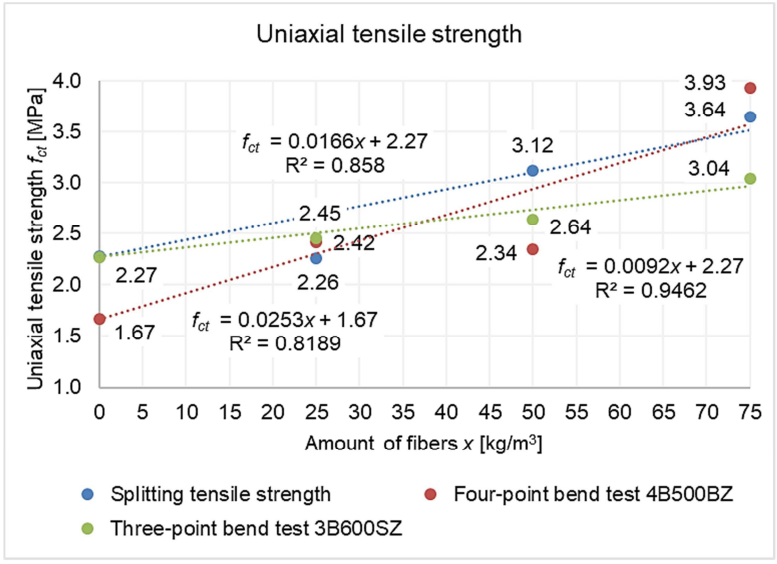

Fig. 22: Uniaxial tensile strength.

The resulting functional dependence (Fig. 23) between the uniaxial tensile strength and the dosing of fibers in concrete is governed by the formula:

$$f_{ct} = 0.017\,x + 2.07 \quad (R^2 = 0.9174), \tag{29}$$

where x is the amount of fibers in kg/m^3.

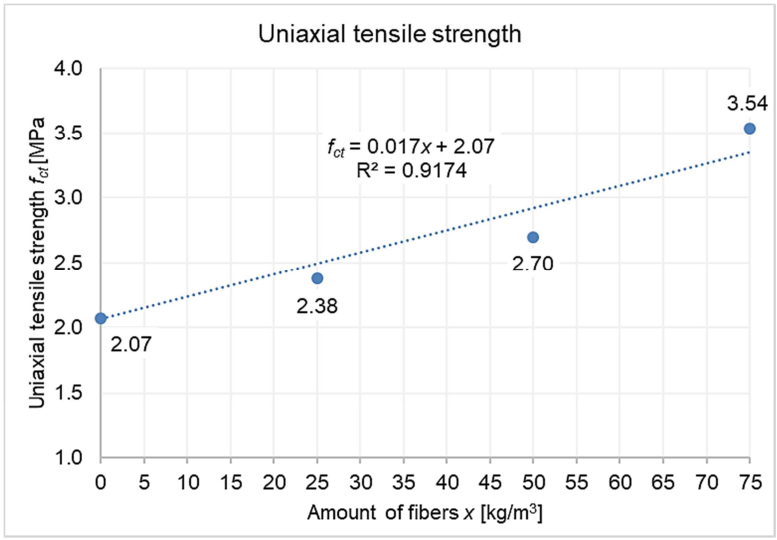

Fig. 23: Uniaxial tensile strength.

6 Numerical modelling

The computed model for four bending test and stress analysis shown in Fig. 24 was created in Scia Engineer 19 [35] with an average size of a finite element 10 mm. The finite element mesh is shown in Fig. 26. The numerical model was created using a 2D member considering beams as a low wall element. A variant solution of a beam simulating a four-point bending test was performed. The variant solution differed by dosing the fibers 0, 25, 50, 75 kg/m^3.

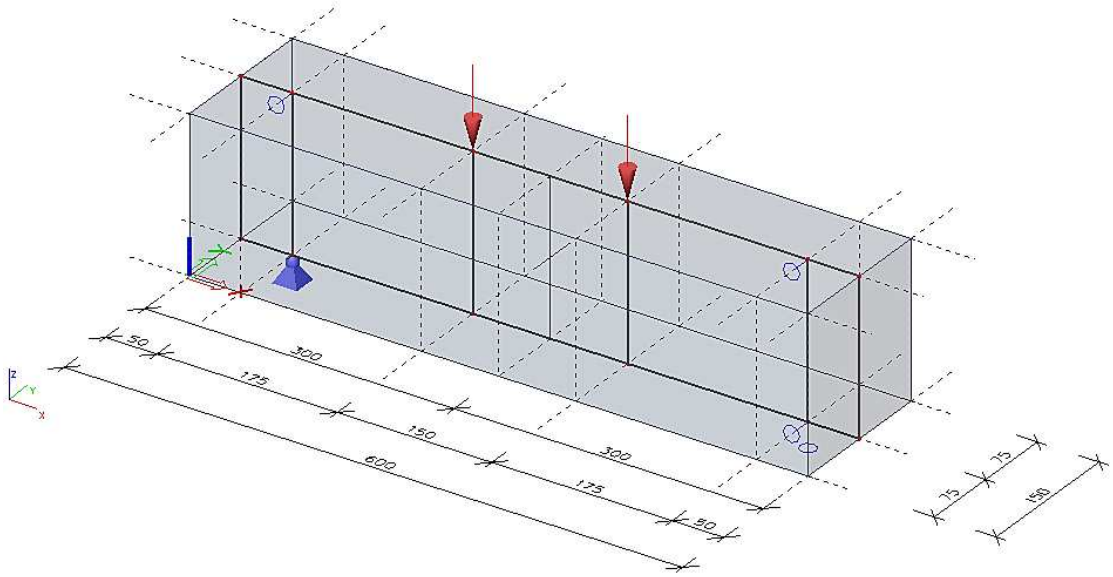

Fig. 24: Scheme four-point bending test.

A linear calculation was performed to determine the normal stresses for dosing 0, 25, 50 and 75 kg/m^3. Normal stress was observed in the centerline of the beam at the load point and in the middle of the span. The results are shown in Table 7. For better orientation in Table 7 shows the coordinates of the nodes in Fig. 25. Results in Table 7 were determined for the decisive peaks of the LD diagram, i.e. the site of the first crack formation and the maximum bearing capacity of the beam (see Fig. 21). Figs. 26 - 29 show the selected results from numerical models for different dosages.

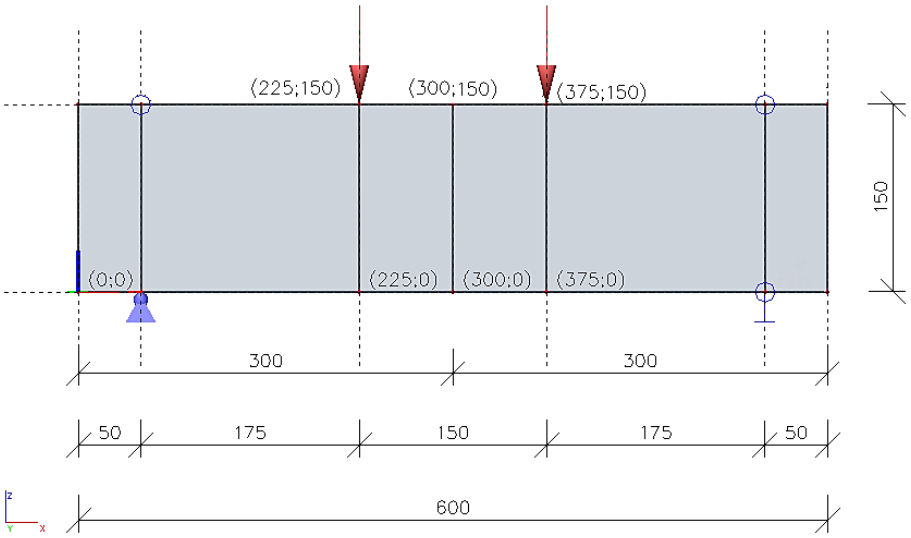

Fig. 25: Four-point test scheme with node designation.

Table 7: Normal stress.

Position		**Normal stress σ_x [MPa]**					
x	**z**	0 kg/m^3	25 kg/m^3	50 kg/m^3	50 kg/m^3	75 kg/m^3	75* kg/m^3
		8.02 kN	13.47 kN	13.00 kN	13.55 kN	11.84 kN	18.99 kN
225	0	2.4	4.1	3.9	4.1	3.6	5.7
225	150	-6.4	-10.7	-10.4	-10.8	-9.4	-15.1
300	**0**	**2.6**	**4.4**	**4.3**	**4.5**	**3.9**	**6.2**
300	**150**	**-2.3**	**-3.9**	**-3.7**	**-3.9**	**-3.4**	**-5.5**
375	0	2.4	4.1	3.9	4.1	3.6	5.8
375	150	-6.3	-10.6	-10.3	-10.7	-9.4	-15

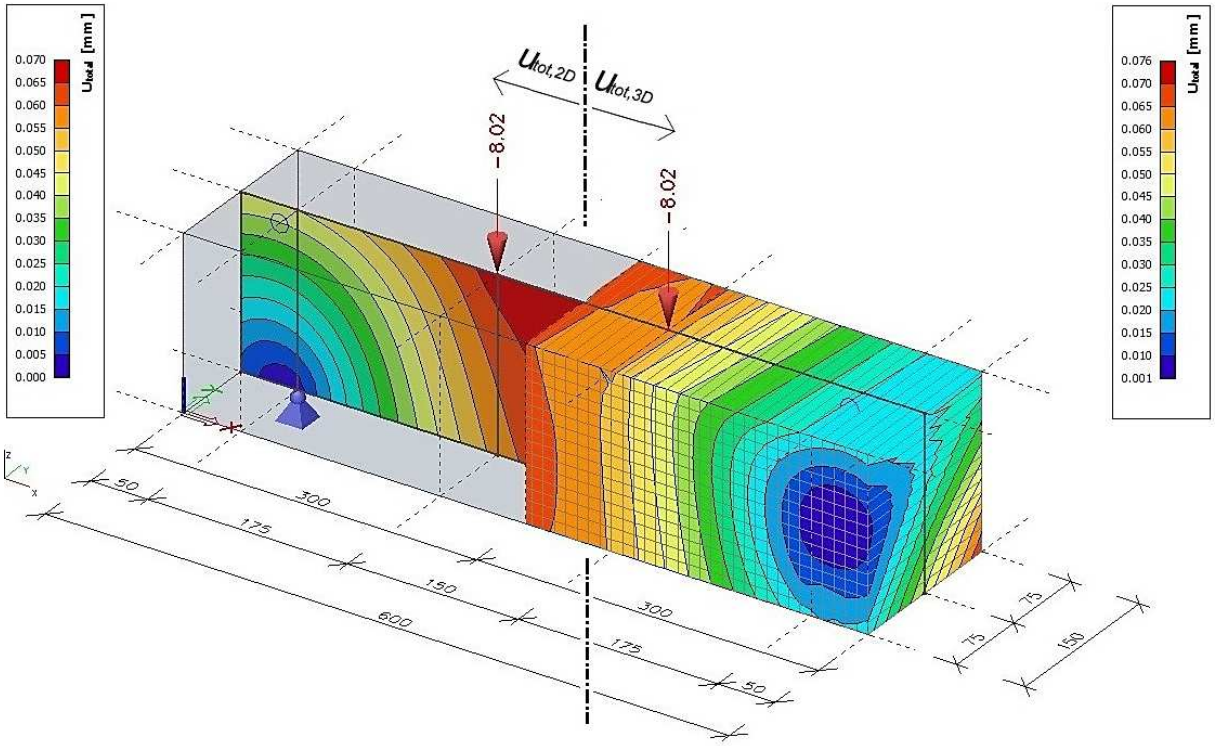

Fig. 26: Displacement for fiber dosing 0 kg/m^3 with force F = 8.02 kN.

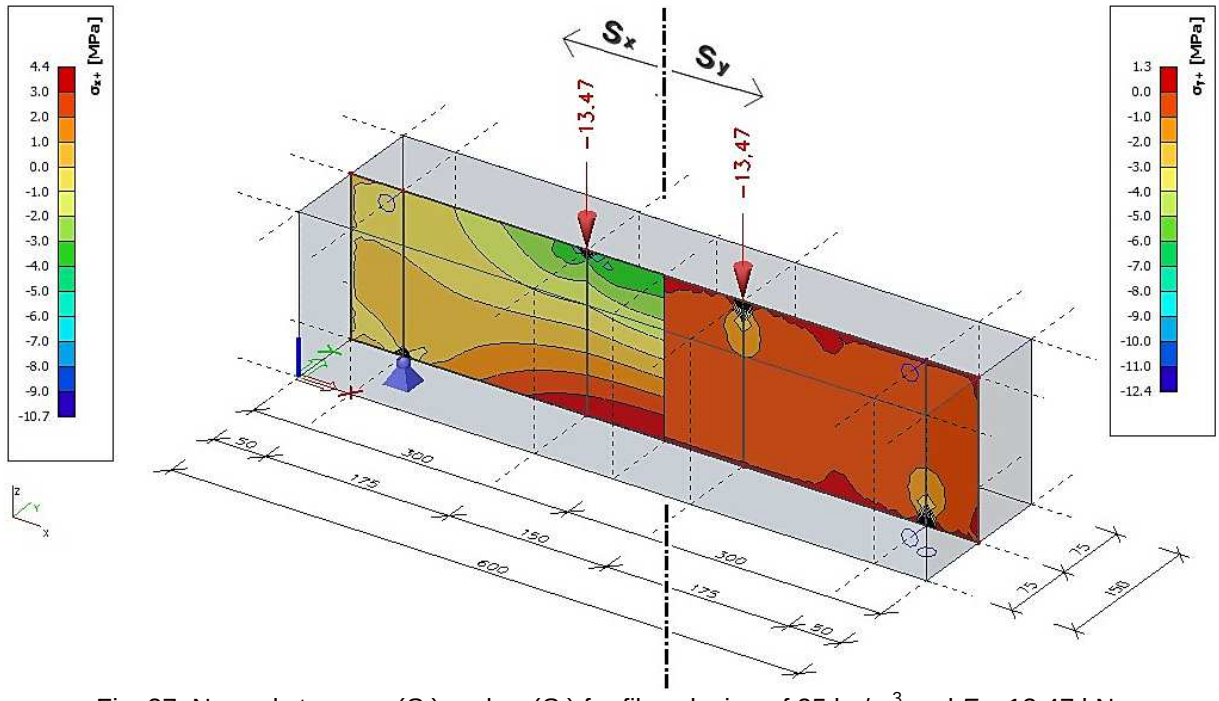

Fig. 27: Normal stress σ_x (S_x) and σ_y (S_y) for fiber dosing of 25 kg/m^3 and F = 13.47 kN.

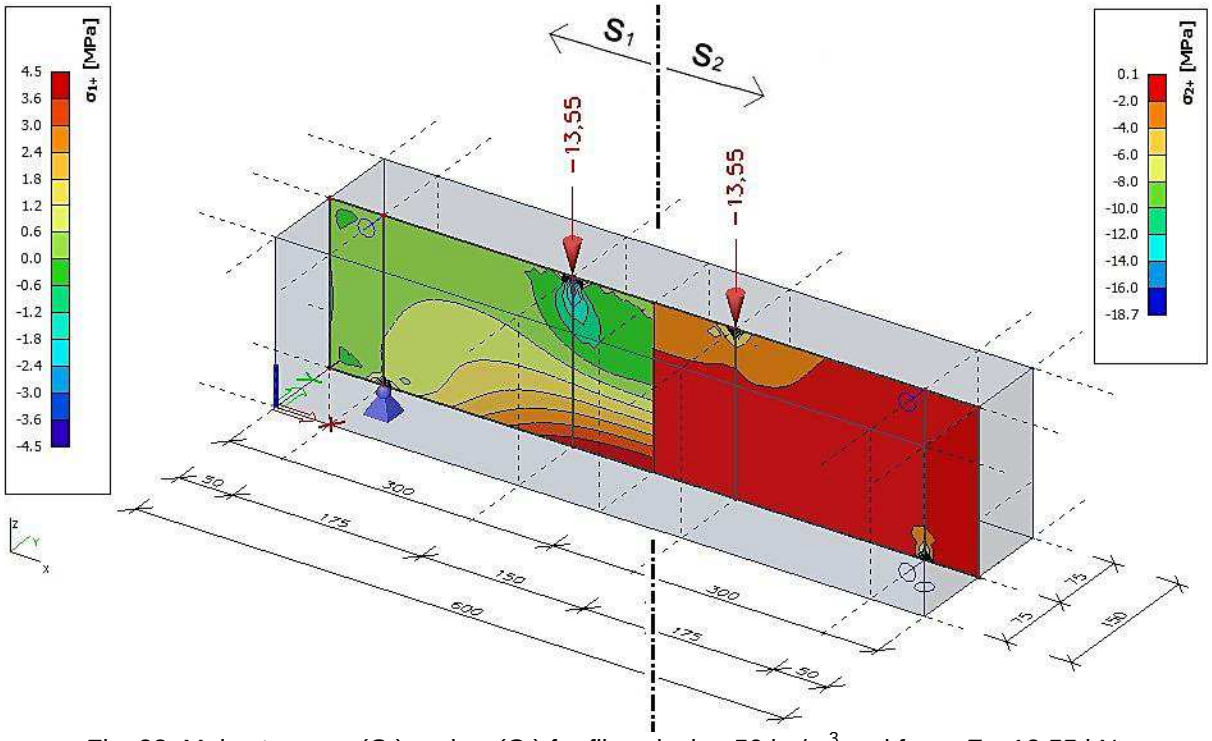

Fig. 28: Main stress σ_1 (S_1) and σ_2 (S_2) for fiber dosing 50 kg/m^3 and force F = 13.55 kN.

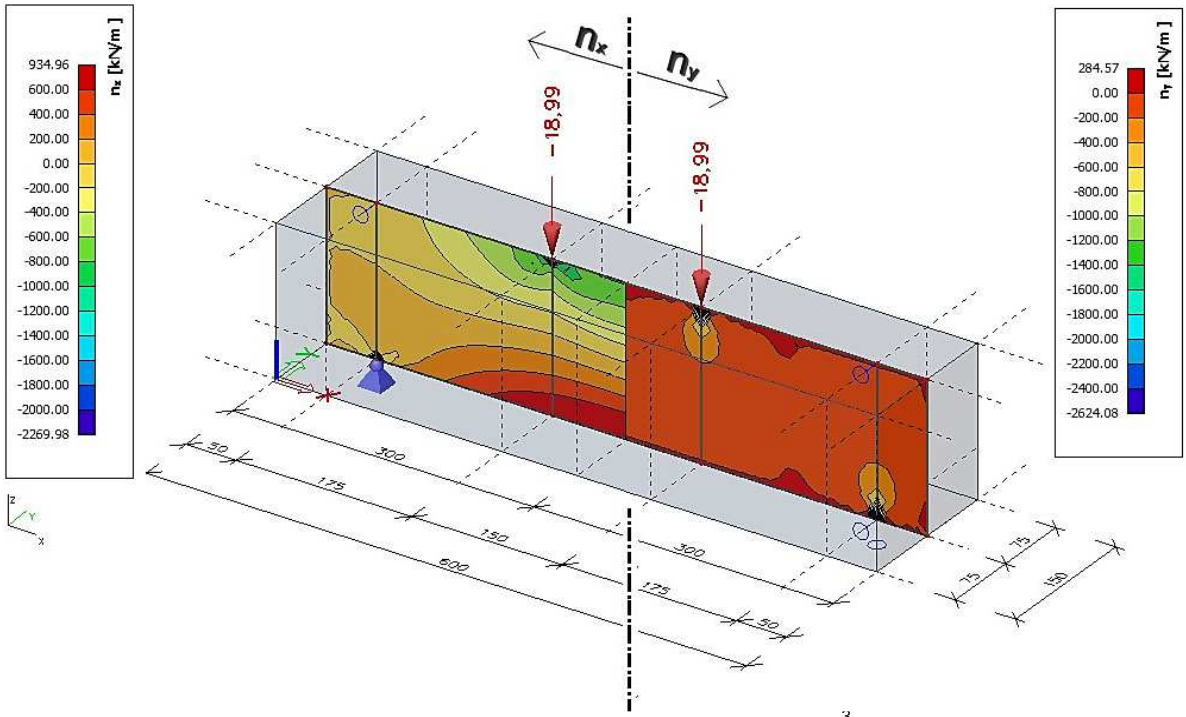

Fig. 29: Normal internal forces n_x and n_y for fiber dosing of 75 kg/m^3 and force F = 18.99 kN.

Furthermore, numerical modelling was performed using 3D calculation model and material model combining concrete and scattered reinforcement. The modeled test included a three-point bend test at a dosage of 75 kg/m^3. The geometry of the computational model and the finite element mesh is shown in Figs. 30 and 31. In the numerical model was used eight-nodal isoparametric finite element. In the middle of the beam was concentrated mesh of finite elements.

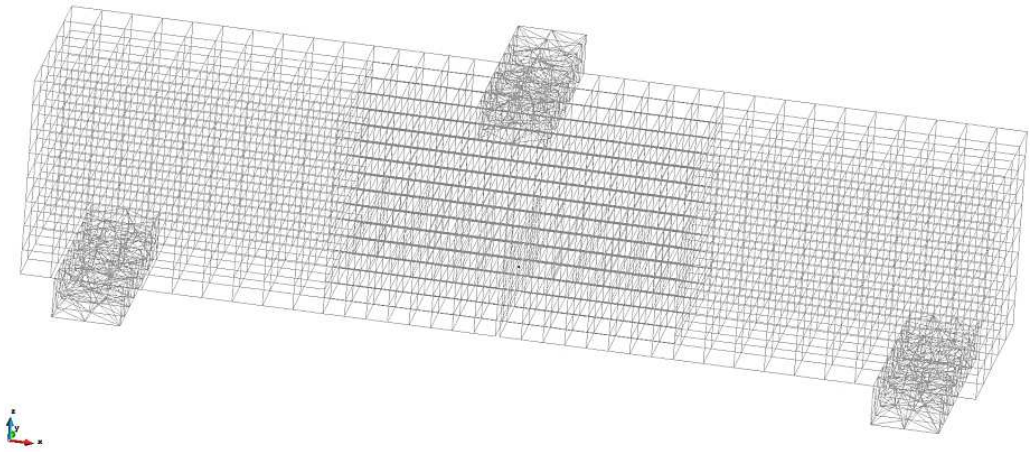

Fig. 30: Numerical model.

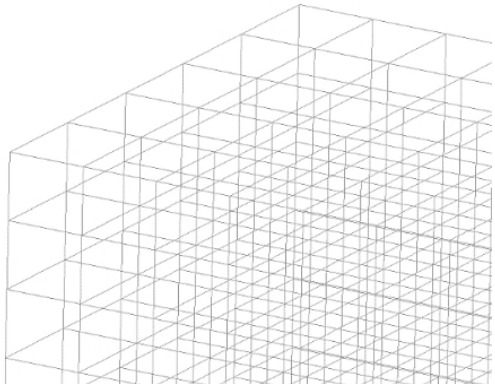

Fig. 31: Detail of finite element mesh for numerical model.

Nonlinear analysis based on the Newton Rapson method was used for the calculation. The deformation load was considered in the calculation. As in the laboratory test. Used material model for concrete is based on the Model Code 2010 recommendation [21]. The material model is fracture - plastic model of concrete [10]. The model uses the theory of fracture mechanics. The modelling was based on recommendations and calculations of concrete structures [36]. The determination of mechanical parameters was based on the procedure and recommendations in [33]. The initial concrete matrix for numerical models has the stated effective mechanical properties in Table 8 and mechanical properties of fibers in Table 9. Fracture energy was calculated from the recommendations for concrete [10].

Table 8: Basic mechanical properties for numerical model.

Compressive strength – cubic $f_{c,cube}$ [MPa]	24.09
Compressive strength – cylindrical $f_{c,cyl}$ [MPa]	20.92
Modulus of elasticity E [GPa]	18.50
Basic tensile strength f_{ct} [MPa]	1.5

When determining the mechanical parameters of the scattered reinforcement, all directions of reinforcement were used equally. The stress-strain diagram was based on the graph shown in Fig. 32.

Table 9: Mechanical properties for numerical model.

Mechanical properties		**ε [-]**
Yield strength f_y [MPa]	1000	-
Tensile strength f_u [MPa]	1050	0.04
Residual strength $f_{residual}$ [MPa]	100	0.45
Coefficient for modulus of elasticity E_{eff} [-]	0.7	-

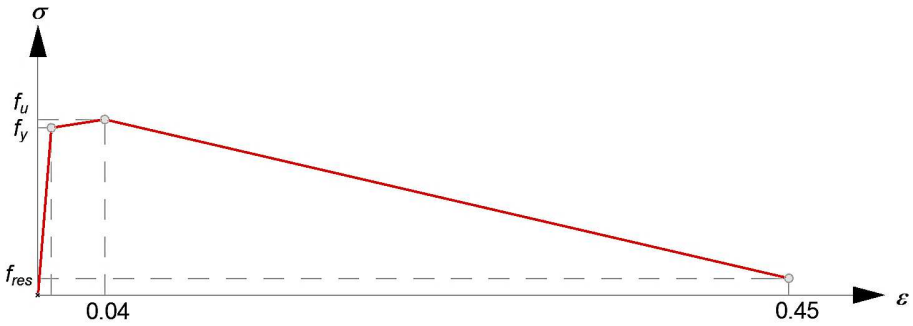

Fig. 32: Stress-strain diagram.

The resulting course of the LD diagram and the tests for the modeled case is shown in Fig. 33.

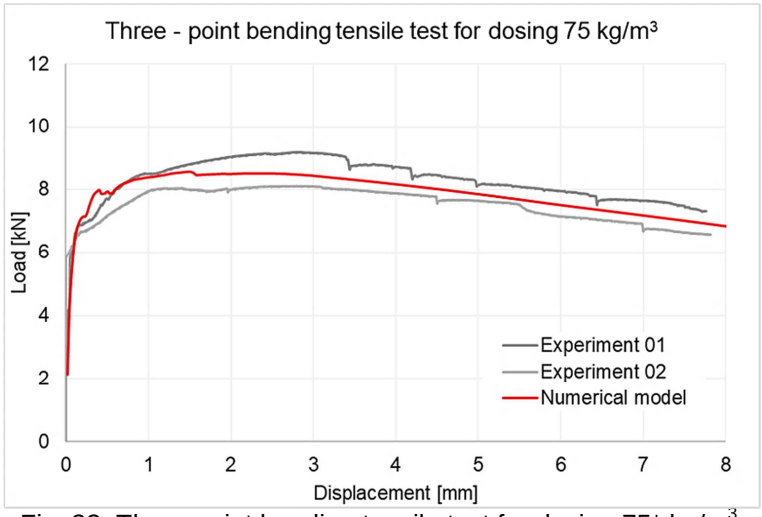

Fig. 33: Three-point bending tensile test for dosing 75* kg/m^3.

The resulting course of the numerical calculation is in very good agreement with the performed tests. The resulting LD diagram from numerical analysis is in most cases in the middle between on the LD diagrams experimentally determined. To illustrate the numerical calculations, the course of normal stresses and cracks in concrete is shown in case of deformation of 1, 5 and 8 mm in Figs. 34 - 36.

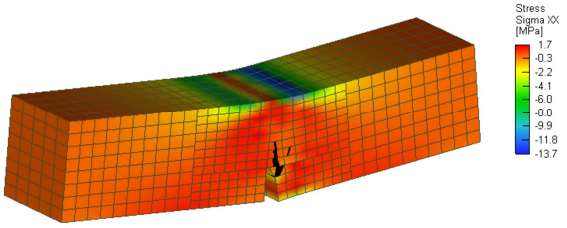

Fig. 34: Normal stress σ_x - displacement 1 mm.

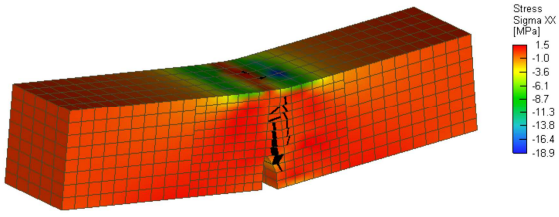

Fig. 35: Normal stress σ_x - displacement 5 mm.

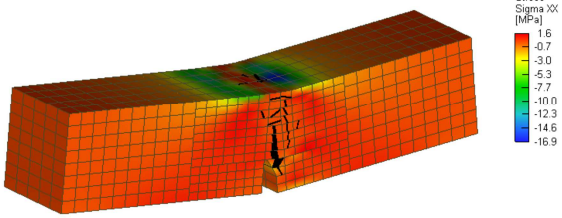

Fig. 36: Normal stress σ_x - displacement 8 mm.

7 Conclusion

The research dealt with the determination of mechanical properties of fiber reinforce concrete for various dosages of fibers in concrete. Specifically, they were fibers Dramix® 3D 65/60 BG with end

bends. Dose fibers was 0, 25, 50, 75 kg/m^3. For a dosage 75 kg/m^3, it has been found that a recipe needs to be adjusted to increase / improve mechanical properties. In some cases, the tensile properties were after the recipe change enlarged up 44 %. The resulting mechanical properties determined based on of laboratory tests are important for numerical modelling, but need to be supplemented with specific parameters as presented for the selected case. Numerical modelling then makes it possible to describe the gradual development of a crack very well and thus to optimize the structural design, e.g. industrial floors, foundation slabs in interaction with the subsoil, etc.

Acknowledgements

This paper has been achieved with the financial support of the Ministry of Education, specifically by the Student Research Grant Competition of the Technical University of Ostrava under identification number SP2019/144.

References

[1] DI PRISCO, M. - COLOMBO, M. - DOZIO, D.: Fibre-reinforced concrete in fib Model Code 2010: Principles, models and test validation. Structural Concrete, Vol. 14, Iss. 4, 2013, pp. 342-361, DOI: 10.1002/suco.201300021.
[2] VASKOVA, J. - CAJKA, R.: Interaction of nonlinear numerical model of SFRC slab and nonlinear numerical subsoil model. International Journal of GEOMATE, Vol. 15, Iss. 47, 2018, pp. 103-110, DOI: 10.21660/2018.47.3576.
[3] SUCHARDA, O. - BILEK, V. - SMIRAKOVA M. - KUBOSEK, J. - CAJKA, R.: Comparative Evaluation of Mechanical Properties of Fibre-Reinforced Concrete and Approach to Modelling of Bearing Capacity Ground Slab. Periodica Polytechnica Civil Engineering, Vol. 61, Iss. 4, 2017, pp. 972-986, DOI:10.3311/PPci.10688.
[4] KATZER, J. - DOMSKI, J.: Quality and mechanical properties of engineered steel fibres used as reinforcement for concrete. Construction and Building Materials, Vol. 34, 2012, pp. 243-248, DOI: 10.1016/j.conbuildmat.2012.02.058.
[5] PONIKIEWSKI, T. - Katzer, J.: Fresh mix characteristics of self-compacting concrete reinforced by fibre. Periodica Polytechnica Civil Engineering, Vol. 61, Iss. 2, 2017, pp. 226-231. https://pp.bme.hu/ci/article/download/9008/7190, DOI: 10.3311/PPci.9008.
[6] SUCHARDA, O. - KONECNY, P. - KUBOSEK, J. - PONIKIEWSKI, T. - DONE, P.: Finite Element Modelling and Identification of the Material Properties of Fibre Concrete. Procedia Engineering, Vol. 109, 2015, pp. 234-239, DOI:10.1016/j.proeng.2015.06.222. http://www.sciencedirect.com /science/journal/18777058.
[7] SAHIN, Y. - KÖKSAL, F.: The influences of matrix and steel fibre tensile strengths on the fracture energy of high-strength concrete. Construction and Building Materials, Vol. 25, Iss. 4, 2011, pp. 1801–1806, DOI: 10.1016/j.conbuildmat.2010.11.084.
[8] SARFARAZI, V. - GHAZVINIAN, A. - SCHUBERT, W. - NEJATI, H.R. - HADEI, R.: A New Approach for Measurement of Tensile Strength of Concrete. Periodica Polytechnica Civil Engineering, Vol. 60, Iss. 2, 2016, pp. 199–203, DOI: 10.3311/PPci.8328.
[9] Report 39: Experimental Determination of the Stress-Crack Opening Curve for Concrete in Tension - Final report of RILEM Technical Committee TC 187-SOC, RILEM Publications, 2007, 41 p., ISBN 978-2-35158-049-3.
[10] CERVENKA, V. - JENDELE, L. - CERVENKA J.: ATENA Program documentation – Part 1: Theory. Cervenka Consulting. Prague, 2018.
[11] BROZOVSKY, J., CAJKA, R., KOKTAN, J.: Constitutive Models for Design of Sustainable Concrete Structures. IOP Conference Series: Earth and Environmental Science, Vol. 143, Iss. 1, 2018.
[12] CERVENKA, V. - CERVENKA, J.: ATENA – A Tool for Engineering Analysis of Fracture in Concrete. “Sadhana” 27(August), 2002, pp. 485–92, DOI:10.1007/BF02706996.
[13] AL-TA 'AN, S.A. – ALSABAWY, A.A.M. - ABDALKADER - AL-GBURI, M. - Al-Ta, S.A.: Nonlinear Finite Element Analysis of Steel Fiber Reinforced, 2015.
[14] KORMANIKOVA, E. – KOTRASOVA, K.: Elastic mechanical properties of fiber reinforced composite materials Chemicke Listy, Vol. 105, Iss. 17.
[15] ZABORSKI, A: Constitutive model for restricted compression of fiber concrete. Cement, Wapno, Beton, Iss. 1, 2016, pp 46-52.
[16] SUCHARDA, O. - BILEK, V.: Aspects of testing and material properties of fiber concrete. Solid State Phenomena, Vol. 292, 2019, pp. 9-14, DOI: 10.4028/www.scientific.net/SSP.292.9.

[17] KOHOUTKOVA, A. - BROUKALOVA, I.: Optimization of Fibre Reinforced Concrete Structural Members. Concrete and Concrete Structures 2013 - 6th International Conference, Book Series: Procedia Engineering, Vol. 65, 2013, pp. 100-106, DOI: 10.1016/j.proeng.2013.09.018.
[18] RILEM (2011): About Rilem [Online], http://www.rilem.net/gene/main.php?base=50017 [Accessed on 4 May 2011].
[19] BS EN 14721: Test method for metallic fibre concrete – Measuring the fibre content in fresh and hardened concrete. BSI, 2005, 2007.
[20] DAfStbguidelines, 2011: DAfStb-Richtlinie Stahlfaserbeton. Deutscher Ausschuss für Stahlbeton - DAfStb, Berlin, Germany (In German).
[21] Model Code 2010 - Final Draft, fib, Bulletin No 65 and 66. 1-2. 2012.
[22] RILEM TC 162-TDF: Test and Design Methods for Steel Fiber Re-inforced Concrete - Design of Steel Fiber Reinforced Concrete Using the σ-w Method: Principles and Application". Materials and Structures/Matériaux et Constructions, Vol. 35, 2002, pp. 262–267. http://www.rilem.org /images/publis/1337.pdf.
[23] RILEM TC 162-TDF: Test and Design Methods for Steel Fiber Reinforced Concrete: σ-ε Design Method, (Chairlady L. Vadewalle). Materials and Structures, Vol. 33, 2000, Iss. 226, pp. 75-81. https://www.rilem.net/images/publis/122603.pdf.
[24] RILEM TC 162-TDF: Test and Design Methods for Steel Fiber Reinforced Concrete: Background and Experiences. Proceedings of the RILEM TC 162-TDF Workshop. (Schnütgen, B., Vandewalle, L. (Eds.)). pp. 222. PRO 031, RILEM Publications S.A.R.L., Bagneaux, 2003.
[25] KRATKY, J. - VODICKA, J. - VASKOVA, J.: Determination of Tensile Part of Fibre Concrete Stress-Strain Diagram from Bending Test Measurements. 5th International Conference Fibre Concrete 2009: Technology, Design, Application, 2009, pp. 167-174.
[26] CAJKA, R. - MANASEK, P.: Building Structures in Danger of Flooding. IABSE Conference New Delhi, India 2005: Role of Structural Engineers towards Reduction of Poverty, 2005, pp. 551-558, ISBN 978-3-85748-111-6, WOS: 000245746100072.
[27] CAJKA, R. - BURKOVIC, K. - BUCHTA, V. - FOJTIK, R.: Experimental Soil – Concrete Plate Interaction Test and Numerical Models. Key Engineering Materials, Vol. 577-578, 2014, pp. 33-36, DOI:10.4028/www.scientific.net/KEM.577-578.33.
[28] AUGUSTÍN, T. - FILLO, L. - HALVONIK, J. - MARCIS, M.: Punching resistance of flat slabs with openings - experimental investigation. Solid State Phenomena, Vol. 272, 2018, pp. 41-46. ISBN: 978-303571284-1, DOI: 10.4028/www.scientific.net/SSP.272.41.
[29] VIDA, R. - HALVONIK, J.: Shear assessment of concrete bridge deck slabs. Key Engineering Materials, Vol. 738, 2017, pp. 110-119, DOI: 10.4028/www.scientific.net/KEM.738.110.
[30] ZIENKIEWICZ, O., C. - TAYLOR, R. L.: The Finite Element Method. Fifth edition, Butterworth-Heinemann, Oxford. 2000, ISBN 0-7506-5049-4.
[31] HOSTETTER, G. - MANG H.A.: Computational Mechanics of Reinforced Concrete Structures. Braunschweig/Wiesbaden: Vieweg-Verlag, 1995, 366 p., ISBN 3-528-06390-4.
[32] KOKTAN, J. - CAJKA, R. - BROZOVSKY, J.: Comparison of 2D and 3D finite element structural analysis of foundation slab on elastic half-space. ARPN Journal of Engineering and Applied Sciences, Vol. 14, Iss. 6, 2019, pp. 1112-1119.
[33] SUCHARDA, O. – PAJAK, M. - PONIKIEWSK, T. - KONEČNÝ, P.: Identification of mechanical and fracture properties of self-compacting concrete beams with different types of steel fibres using inverse analysis. Construction and Building Materials. Vol. 138, Iss. 5, 2017, pp. 263-275, DOI: 10.1016/j.conbuildmat.2017.01.077.
[34] Bekaert. https://www.bekaert.com/en/products/construction/concrete-reinforcement.
[35] Scia Engineer 19. https://www.scia.net/cs.
[36] SUCHARDA, O. - KONEČNÝ, P.: Recommendation for the modelling of 3D non-linear analysis of RC beam tests. Computers and Concrete, Vol. 21. Iss. 1, 2018, pp. 11-20, DOI: 10.12989/cac.2018.21.1.011.